NANO LETTERS

Letter

pubs.acs.org/NanoLett

The Role of Electronic and Phononic Excitation in the Optical Response of Monolayer WS_2 after Ultrafast Excitation

Claudia Ruppert,*[,†,‡,▽] Alexey Chernikov,[†,§,▽] Heather M. Hill,[†,∥,⊥] Albert F. Rigosi,[†,∥,⊥] and Tony F. Heinz[†,∥,⊥]

[†]Departments of Physics and Electrical Engineering, Columbia University, New York, New York 10027, United States

[‡]Department of Physics, Technische Universität Dortmund, Dortmund 44227, Germany

[§]Department of Physics, University of Regensburg, Regensburg 93053, Germany

[∥]Department of Applied Physics, Stanford University, Stanford, California 94305, United States

[⊥]SLAC National Accelerator Laboratory, Menlo Park, California 94025, United States

ABSTRACT: Transient changes of the optical response of WS_2 monolayers are studied by femtosecond broadband pump−probe spectroscopy. Time-dependent absorption spectra are analyzed by tracking the line width broadening, bleaching, and energy shift of the main exciton resonance as a function of time delay after the excitation. Two main sources for the pump-induced changes of the optical response are identified. Specifically, we find an interplay between modifications induced by many-body interactions from photoexcited carriers and by the subsequent transfer of the excitation to the phonon system followed by cooling of the material through the heat transfer to the substrate.

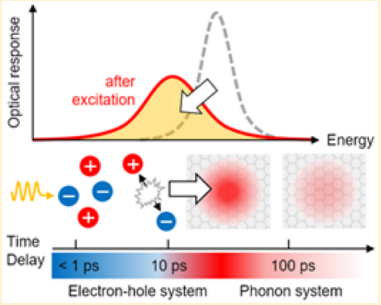

KEYWORDS: *Atomically thin 2D materials, ultrafast spectroscopy, carrier and phonon dynamics*

Atomically thin materials have received much recent attention from the scientific community. Particular interest has been directed toward the family of semiconducting transition metal dichalcogenides (TMDCs),[1−3] including MoS_2, WS_2, $MoSe_2$, WSe_2, and $MoTe_2$ crystals. This class of materials is characterized by intriguing physical properties, including strong Coulomb interactions and distinctive spin-valley physics.[4−9] TMDC materials offer excellent opportunities to study fundamental phenomena in condensed matter as well as to explore properties important for future applications. Within this context, it is crucial to understand how these systems respond to external perturbations. Recent efforts have been directed toward studying the response of mono- and few-layer TMDCs to optical excitation, particularly focusing on the behavior of the photoexcited charge carriers. A variety of distinct phenomena have been explored, including photoexcited carrier lifetimes,[10−17] exciton−exciton interactions and annihilation processes,[18−21] coherent coupling and control,[22−24] bandgap renormalization,[25−28] behavior in the high-density regimes beyond the Mott threshold,[29] ultrafast structural deformation,[30] and spin-valley dynamics.[31−38] In the majority of these studies, ultrafast optical pump−probe spectroscopy was utilized as a useful experimental tool. Pump-induced changes of the optical response can, however, be challenging to analyze because even an isolated resonance can exhibit nontrivial modifications after the photoexcitation. In addition, both photoexcited charge carriers and nonequilibrium phonon populations (including transient heating of the lattice) can alter the optical properties of the material.

In this letter, we address this issue by presenting a detailed analysis of the evolution of the exciton line shape after photoexcitation of a WS_2 monolayer using femtosecond broadband pump−probe spectroscopy. From our data, we extract individual contributions to the modification of the optical response—namely, changes in the exciton peak area, line width, and energy—and monitor their temporal evolution. Such a deconvolution of the different contributions allows for a more detailed analysis of the optical response after the excitation and facilitates the analysis of the underlying physical processes. Through this approach, we identify two different regimes. The first regime is dominated by the many-body interactions originating from the optically injected charge carriers during roughly the first 1−10 ps of the excitation for the chosen intermediate pump densities, and the second later regime is strongly influenced by the transfer of electronic excitation to phonons. In particular, we demonstrate that the resulting transient increase of the lattice temperature is largely sufficient to account for the observed changes of the optical response after the majority of the photoexcited electron−hole pairs have recombined. The subsequent decay of the pump−probe signal on the 100 ps time scale is attributed primarily to the cooling of the phonon system by thermal coupling to the underlying substrate.

Received: August 20, 2016
Revised: December 16, 2016
Published: January 6, 2017

DOI: 10.1021/acs.nanolett.6b03513
Nano Lett. 2017, 17, 644−651

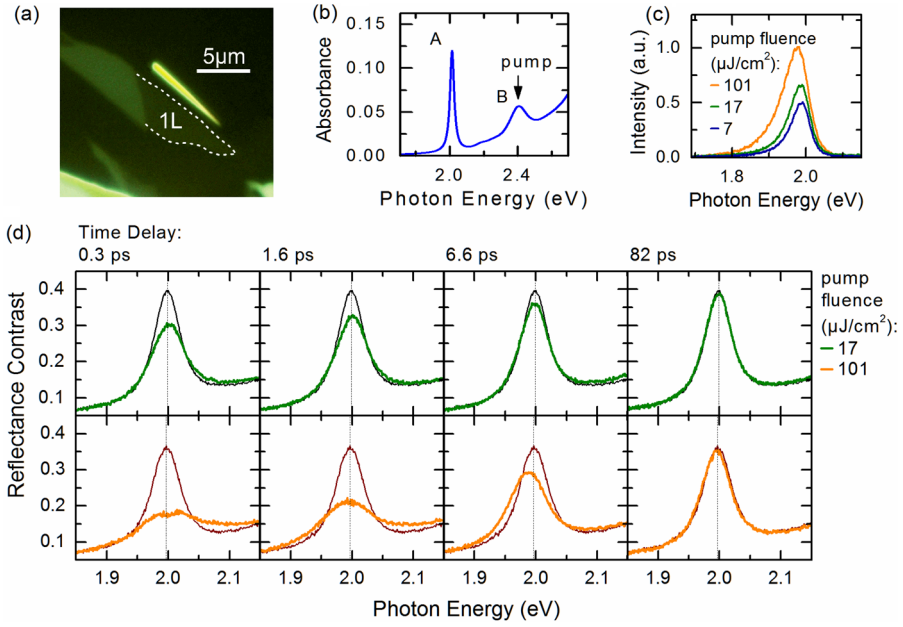

Figure 1. Spectrally resolved pump−probe measurements of a WS_2 monolayer. (a) Optical micrograph of the studied WS_2 flake on a fused silica substrate. The monolayer region is indicated by the dotted line. (b) A typical linear absorbance spectrum of a WS_2 monolayer on a fused silica substrate (data from ref 39) in the spectral range of the A and B transitions. The arrow indicates the photon energy of the pump radiation used in the pump−probe experiment. (c) Photoluminescence spectra of the sample shown in (a) for three different pump fluences. (d) Room-temperature reflectance contrast spectra at selected delay times after the excitation for the pump fluencies of 17 μJ/cm^2 (top panel) and 101 μJ/cm^2 (bottom panel). Spectra before the pump (Δt = −0.4 ps) are also plotted for comparison (dark thin lines) illustrating the response prior to excitation.

The WS_2 monolayer sample was prepared by mechanical exfoliation of a synthetic bulk crystal onto a fused silica substrate. The corresponding optical micrograph is presented in Figure 1(a), where the monolayer area is indicated by a dashed line. In our experiment, the sample was excited by a frequency-doubled, amplified fiber laser with pulses of ∼250 fs duration and a repetition rate of 1 MHz, centered at the photon energy of 2.4 eV. The changes in the optical response were probed by white-light supercontinuum pulses generated in a YAG crystal by pump pulses at the fundamental frequency of the modelocked laser. Both pump and probe beams were focused onto the sample in collinear geometry by a microscope objective, yielding respective spot sizes of 5 and 2 μm, and a mechanical delay stage was used to control the time delay Δt between the pulses. The reflected probe signal was spectrally dispersed in a spectrometer and detected by a charge-coupled device array. We adopted a balanced detection scheme with a reference white-light pulse being measured simultaneously to compensate for fluctuations in the intensity of the probe beam. The data were corrected for the wavelength-dependent chirp of the supercontinuum probe pulses, which was measured using the ultrafast response of a thin gold foil. All measurements were performed at room temperature and under ambient atmosphere.

The excitation conditions are further illustrated in Figure 1(b), where a typical absorption spectrum of a supported WS_2 monolayer (from ref 39) is presented. The spin-split exciton ground-state resonances corresponding to the direct transition at the K/K′ point of the Brillouin zone are labeled as A and B. The pump photon energy of 2.4 eV, indicated by the arrow in Figure 1(b), predominantly leads to the optical injection of electron−hole pairs at the B exciton resonance with smaller contributions from the electron-hole continuum of the A transition and from the flank of the higher-lying states.[40,41] The applied pump fluence F was varied from 7 to 101 μJ/cm^2, corresponding to the photoexcited electron−hole pair densities between 9 × 10^{11} and 1.3 × 10^{13} cm^{-2}, as estimated from the absorbance of ∼0.05 at the pump photon energy (see Figure 1(b)). This density range can be considered an intermediate excitation regime, where the interactions between the charge carriers already play a significant role, yet excitons are still bound states, i.e., the densities are below the so-called Mott threshold, where excitons dissociate.[25,26,29] Optical excitation of such monolayer samples supported on a substrate can give rise to changes in the charge state of the layer through photodoping effects with corresponding modifications of the optical response[42] associated with charged exciton states.[43,44] However, for our samples exposed to air at room temperature, such optically induced doping was shown to be significantly reduced.[42] In addition, because of the observed line shape of the resonance and the absence of a second peak in the reflectance contrast,[26] we conclude that the optical response in our experiment is governed by neutral excitons. The fluence of the probe beam was kept sufficiently low (∼1 μJ/cm^2) to be nonperturbative with induced carrier densities at least an order of magnitude lower than the density created by the pump.

In the following, we focus on the optical response at the fundamental optical gap, i.e., A exciton resonance. We use the reflectance contrast RC = $(R_{WS_2+S} - R_S)/R_S$ as the main observable, where R_{WS_2+S} and R_S denote the reflectance of the WS_2 monolayer on the substrate and of the bare substrate, respectively. Fused silica was the substrate of choice as there are no complex interference effects influencing the reflectance contrast spectra, as would occur for substrates such as silicon covered by a thin film of thermal oxide. Furthermore, for a transparent substrate covered by an ultrathin layer producing a moderate reflectance contrast signal, the reflectance contrast is

DOI: 10.1021/acs.nanolett.6b03513
Nano Lett. 2017, 17, 644−651

mostly determined by the imaginary part of the dielectric function, i.e., by the sample absorption.[39]

The photoluminescence (PL) of the WS_2 monolayer under femtosecond pulsed laser excitation is shown in Figure 1(c) for different fluences. For low pump fluences, the maximum of the PL feature lies at 1.986 eV, but shifts to slightly lower energies with increasing pump fluence. This phenomenon is linked to the pulsed nature of the excitation, as described in detail below. The PL peak follows this trend because most of the photons are emitted on a time scale comparable to the duration of the spectral shift of the resonance. The overall shape of the PL feature and its energy corroborate the assumption that the optical response is governed by neutral excitons.

Reflectance contrast spectra of the WS_2 monolayer are presented in Figure 1(d) at selected time delays after the excitation with low (17 μJ/cm, top panels) and high (101 μJ/cm^2, bottom panels) pump fluences. A spectrum at negative time delay is included in each panel for comparison. For both fluences, the pump-induced modification of the exciton resonance is a combination of changes in the line width, area, and energy of the peak. In particular, both blue and red shifts of the resonance are observed. (See, e.g., spectra at Δt = 0.3 ps for F = 17 μJ/cm^2 and at Δt = 6.6 ps for F = 101 μJ/cm^2 in Figure 1(d).)

We repeated the measurements on a second monolayer of WS_2 in the vicinity of the specimen shown in Figure 1(a). We obtained very similar results from the second sample as those described above. Furthermore, environmentally induced changes of the optical response seem to be of minor importance under our measurement conditions. We performed the experiment under vacuum conditions without a meaningful difference in the experimental findings. We note that this comparison does not imply that interactions of the WS_2 monolayer with the substrate are unimportant because the same substrate was used throughout.

To extract the individual contributions to the induced spectral changes, we performed a line shape analysis of the data in Figure 1(d) by fitting a Lorentzian function to the A exciton peak with a linear offset to account for the broad background, as illustrated in Figure 2(a). This allows us to monitor the pump-induced changes in the peak line width w (full-width at half-maximum), the area A, and the resonance energy E independently as a function of delay time after excitation. The extracted parameters are presented in Figure 2(b) for a pump fluence of 101 μJ/cm^2. The data are normalized to the corresponding values at negative time delays: w_0 = 47 meV, A_0 = 1 arb unit, and E_0 = 1.996 eV. These latter parameters differ only very slightly from the ones obtained in the absence of the pump beam, indicating the absence of any appreciable steady-state heating of the sample by the pump beam. For direct comparison, the change of the normalized reflectance contrast $\Delta RC/RC_0$ at the peak of the resonance (integrated over a narrow spectral region of 13 meV) is presented in the lower panel of Figure 2(b). This temporal evolution, which might be recorded in a more conventional pump–probe measurement at fixed probe wavelength, reflects a complex combination of the individual dynamics arising from peak shifts, broadening, and a decrease of the peak area.

Changes in the optical response of the WS_2 monolayer appear immediately after pump excitation within the experimental resolution of several 100s of femtoseconds. Initially, we observe a strong increase of the line width of A exciton, accompanied by a simultaneous bleaching of the resonance, i.e., a decrease in the area of the feature. Both the broadening and bleaching of the feature exhibit decay dynamics on the picosecond time scale (inset of Figure 2(b)). After a few 10s of ps, the peak area returns to its original value, and the optical response mostly reflects a red shift of the exciton transition energy with only a small contribution from line width broadening. These changes then decay on the 100 ps time scale, and the system fully recovers after ~250 ps. In the following, we analyze the two regimes of fast and slow dynamics in detail, examining both the origin of the individual contributions and their associated time constants.

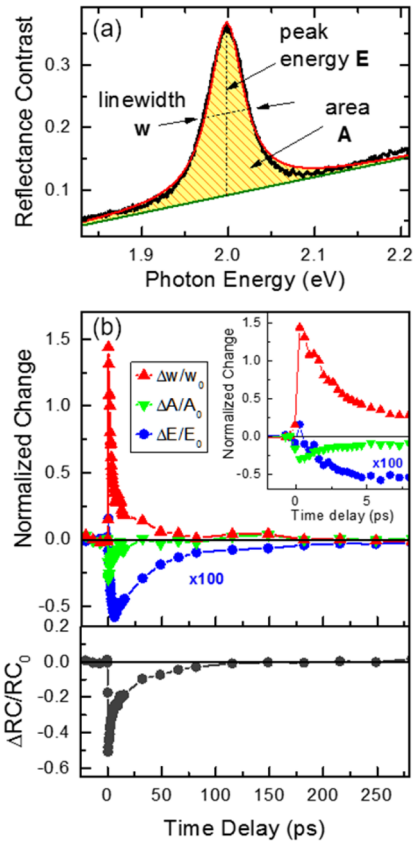

Figure 2. Quantitative analysis of the time-dependent line shape of the A exciton resonance. (a) Representative reflectance contrast spectrum fitted with a Lorentzian line shape (red line) and linear offset (green line). (b) Relative changes of the line width $\Delta w/w_0$, area $\Delta A/A_0$, and resonance energy $\Delta E/E_0$ of the peak are presented as a function of time delay for a pump fluence of 101 μJ/cm^2. The data are normalized to the corresponding values at negative delay times: w_0 = 47 meV, A_0 = 1 arb unit, and E_0 = 1.996 eV. (inset) The relative change of the line width and area for short delay times. Lower panel: The relative change of the reflectance contrast RC at a probe energy of 1.997 eV, averaged over a narrow spectral range of 13 meV, is shown for comparison.

We begin with a discussion of the photoinduced optical response on fast time scales. Initially, the optical pulse creates electron–hole pairs at the excitation photon energy. The subsequent scattering processes with phonons and with other carriers are expected to lead to rapid thermalization and relaxation of the carrier population toward the respective band minima. For nonresonant excitation processes corresponding to the experimental conditions in our study, the time scales for this initial relaxation are usually expected to be on the order of 100s of femtoseconds[45] and should thus be below the resolution of our measurements. The presence of the

DOI: 10.1021/acs.nanolett.6b03513
Nano Lett. 2017, 17, 644–651

photoexcited carriers in the material strongly modifies the optical response at the exciton resonance. Several distinct physical processes contribute to this response.[25,38,46] First, Coulomb scattering of the carriers leads to the spectral broadening of the exciton peak, a process usually termed excitation-induced dephasing. Second, phase-space filling (or Pauli-blocking) of the electron and hole states, as well as the screening of the Coulomb interaction, results in reduced exciton binding energy and oscillator strength. The latter manifests itself in a decrease of the exciton peak area and, thus, bleaching of the resonance. Third, the quasi-particle band gap energy, i.e., energy of the onset of the electron−hole continuum, decreases due to the reduction of repulsive Coulomb interactions. Combined with the decreased exciton binding energy from phase-space filling and screening, this can lead to a shift of the exciton resonance either to higher or lower energy. We note that the resulting absolute energy shift of the resonance generally depends on a variety of material properties and excitation conditions, including the effective temperature and density of the photoexcited carriers, as well as the ratio of the excitons to free electrons and holes.

A comprehensive many-body theoretical approach is typically required for an accurate, quantitative description of the phenomena outlined above. Nevertheless, the overall changes in the optical spectra, such as the simultaneous broadening and bleaching of the exciton resonance, allow us to identify the initial response as arising from the presence of photoexcited carriers and to monitor their dynamics.

With this qualitative description of the initial transient optical response, we now turn to a closer examination of the parameters obtained in our experiment. The extracted changes of the line width, area, and energy of the exciton resonance during the first 10 ps are presented in Figure 3(a−c) for the pump fluences of 17 and 101 μJ/cm^2. The observed line width broadening (Figure 3(a)) and bleaching (Figure 3(b)) of the exciton resonance are strongly correlated with one another and both scale with pump fluence. As discussed above, both observations are consistent with the influence of the photoexcited carriers. In particular, the measured absolute magnitude of the excitation-induced broadening of $6.3(\pm1) \times 10^{-12}$ meV cm^{-2} carriers compares well to the results for a similar monolayer material (MoS_2) studied under comparable experimental conditions[21] and to a reported value of 5.4×10^{-12} meV cm^{-2} for exciton−exciton scattering in WSe_2 monolayers.[16] As discussed in detail in ref 16, the large magnitude of the carrier-induced broadening, compared to typical III−V and II−VI quantum well systems, reflects the unusually strong Coulomb interaction in TMDC monolayer materials. In addition, the maximum measured bleaching of ∼30% at the highest pump fluence is consistent with the electron−hole densities lying below the Mott threshold.[25,29,46] We also note that because both phase-space filling and Coulomb screening give rise to a bleaching signal, it is usually difficult to distinguish the two contributions. However, recent reports[25,26,38] including a strong modification of the optical response from the presence of free electrons in the spin-split lower conduction band in WS_2[26] (which does not contribute to the formation of the optically bright A exciton state), indicate the existence of significant contributions from screening in TMDC monolayers.

In addition to pump-induced broadening and bleaching, we observe an instantaneous blue shift of the exciton resonance immediately after the excitation, which subsequently turns into

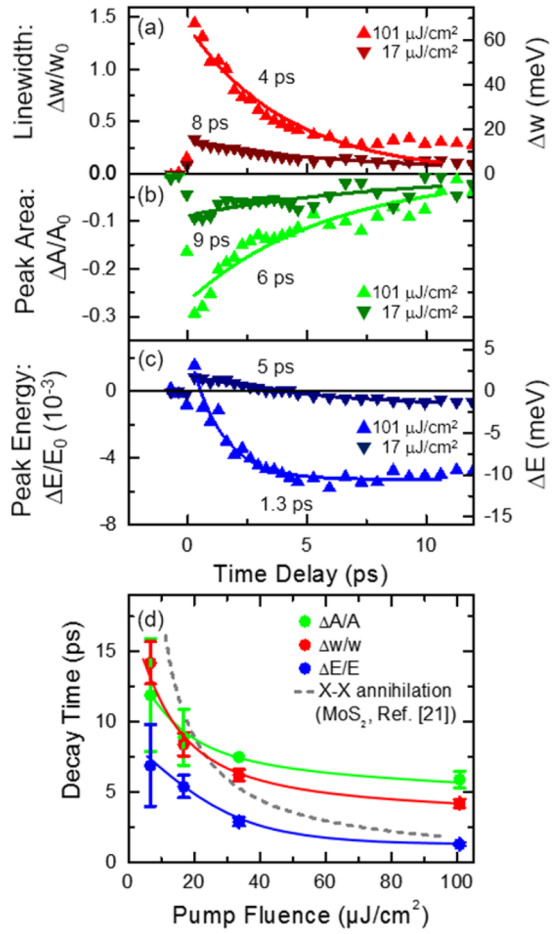

Figure 3. Pump−probe dynamics on short time scales after the excitation as governed by the excited carrier population. Relative changes of the line width (a) $\Delta w/w_0$, (b) area $\Delta A/A_0$, and (c) energy $\Delta E/E_0$ of the A exciton feature for the pump fluences of 17 and 101 μJ/cm^2. Also shown are single exponential fits (solid lines) used to quantify the time scale of the initial decay and the resulting time constants. The extracted time constants as a function of pump fluence are presented in (d). The solid lines are guides to the eye. The corresponding initial decay times from exciton−exciton annihilation in MoS_2 monolayers (ref 21) are added for comparison and are represented by the dashed gray line.

a red shift. The relative magnitude of the blue shift is small compared to the changes in the line width and peak area. As previously discussed, the shift of the exciton resonance due to the presence of carriers involves a subtle interplay between the reduction of the exciton binding energy and the renormalization of the quasi-particle band gap. Although the former leads to a decreased exciton binding energy, resulting in a blue shift of the exciton resonance, the latter leads to a smaller band gap and thus contributes to a red shift of the optical transitions. A blue shift of the exciton peak under nonequilibrium conditions in monolayer TMDCs was previously reported for optically excited[18] and electrostatically gated samples.[26,43,47] Many-body calculations, however, predict an effective red shift in the presence of free electrons and holes for all but the lowest densities for the case of MoS_2 monolayers.[25] The precise microscopic origin of the shift due to the presence of excited carriers may thus strongly depend on the specific conditions, including the ratios of bound and unbound electron−hole pairs, carrier temperature, and so forth. Nevertheless, the decay of the

DOI: 10.1021/acs.nanolett.6b03513
Nano Lett. 2017, 17, 644−651

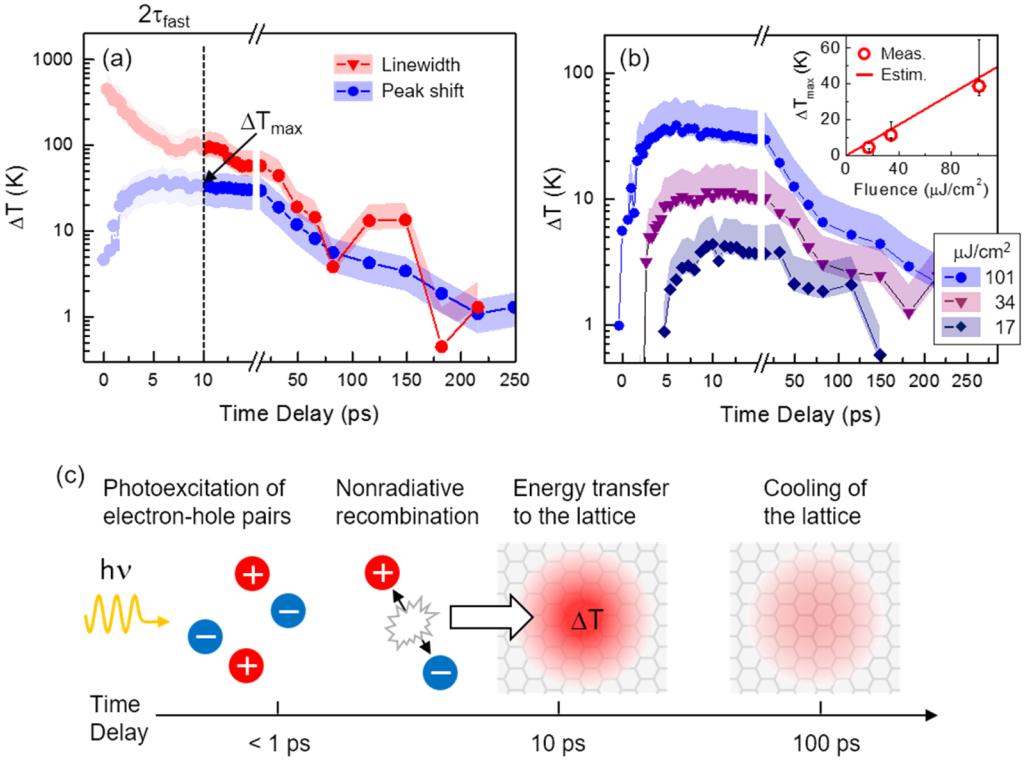

Figure 4. Pump–probe dynamics on longer time scales: decay of the carrier population followed by heating and subsequent cooling of the lattice. (a) Increase of the lattice temperature ΔT as extracted from the shift of the peak energy and from broadening of the line width for a pump fluence of 101 $\mu J/cm^2$. Time constant for recombination of the photoexcited carriers and the maximum temperature increase are denoted by τ_{fast} and ΔT_{max}, respectively. (b) Comparison of the temperature transients extracted from the shift of the peak energy for three different pump fluences. Corresponding maximum temperature increases ΔT_{max}, and the results of the estimate based on heat capacity are presented in the inset. (c) Schematic illustration of the overall scenario after pulsed optical excitation of the WS_2 monolayer, consistent with the observed photoinduced changes in the optical response.

blue shift and the development of the red shift roughly coincide with the decay of the photoinduced broadening and bleaching signals. Therefore, we can tentatively attribute the blue shift to the presence of photoexcited carriers under the experimental conditions of our study.

To analyze the carrier dynamics, we compare the time scales of the initial decay, extracted by exponential fitting of the individual contributions in Figure 3(a–c) and presented in Figure 3(d), as a function of pump fluence. As previously noted, the changes in the peak line width, area, and energy are strongly correlated with one another. The corresponding time constants are slightly below 15 ps for the lowest fluence and decrease with increasing fluence down to several picoseconds. We can thus exclude radiative recombination at room temperature of thermalized excitons and free electron–holes due to the short, picosecond time scales (theoretical predictions for effective radiative recombination are in the nanosecond range[48,49]) and the low quantum yield of the as-exfoliated TMDC samples.[2,50] In addition, scattering of bright excitons to optically dark states due to the conduction band spin-splitting in monolayer TMDCs[51] is expected to occur on time scales of a few picoseconds.[52] Although this process is typically accompanied by a decrease in the photoluminescence from the sample,[52,53] it should not lead to a strong modification of the reflectance contrast because Coulomb-scattering, screening, and Pauli-blocking from the photoexcited holes should contribute to changes of the bright and dark exciton states in a similar manner.[38] Nonradiative recombination via defects and Auger-type exciton–exciton annihilation[19−21] are therefore considered to be the dominant decay channels. The observed decrease of the recombination time with increasing pump density as well as the comparison of the initial decay constants with the density-dependent Auger rates from a recent study on MoS_2,[21] presented in Figure 3(d) as a dashed line, supports the latter mechanism. Overall, the initial transient changes of the optical response at short time scales, <10 ps, after the excitation are attributed to the presence of photoexcited carriers and their subsequent nonradiative decay via Auger processes.

Next, we consider the regime of slower dynamics. A number of studies in the literature attribute the optical response at longer delay times to the influence of charge carriers with corresponding lifetimes. In many cases, at delay times longer than ∼100 ps, a finite carrier population is indeed still present in the system, as observed in time-resolved photoluminescence measurements.[10,52] Nevertheless, as we show in the following, thermal effects can play a particularly important role in pump–probe absorption-type experiments, as the changes in the optical response at later time-scales can be explained largely by phonon dynamics, i.e., by heating and subsequent cooling of the lattice.

Because the main recombination channel for the photoexcited carriers in currently available TMDC monolayers is usually nonradiative, as is the case for WS_2, it is reasonable to conclude that the energy of the pump pulse is largely transferred from the carrier to the phonon system. In particular, for an Auger-type annihilation mechanism, where an electron–hole pair recombines by exciting a second electron–hole pair to a higher lying state, the excess energy of the second pair is

DOI: 10.1021/acs.nanolett.6b03513
Nano Lett. 2017, 17, 644–651

rapidly converted to phonons as it relaxes toward the band edge. In this case, the energy transfer rate to the phonon system is expected to roughly match the effective annihilation rate so that the recombination of optically injected carriers correlates with the increase of the phonon population. The energy is expected to be subsequently transferred from optical to acoustic phonons within a few picoseconds.[54,55] On these time scales, the thermalization of the phonons should thus roughly follow the energy dissipation of the photoexcited carriers. Most importantly, the resulting heating of the lattice modifies the optical response of the material by shifting the exciton peak position to lower energies in accordance with the temperature-dependent shift of the band gap and by introducing an additional line width broadening mechanism from increased carrier-phonon scattering rates. Previous temperature-dependent studies of TMDC monolayers allow us to relate the measured shift and broadening in a semiquantitative fashion to the lattice temperature. In general, both the temperature-dependent shift and the line width of the resonance can exhibit nontrivial temperature dependence. In many cases, however, including mono- and few-layer TMDCs, the scaling of the shift and broadening can be reasonably approximated by a linear relationship for not too large temperature changes at elevated temperatures, such as room temperature and above. For various monolayer TMDCs, we find literature values for the temperature-dependent shift of the exciton resonance energy lying between −0.26 and −0.5 meV/K (most values are closer to −0.3 meV/K) and for the line width increase lying between 0.12 and 0.25 meV/K. These estimates of the coefficient reflect either published temperature variation or were determined by directly analyzing temperature-dependent photoluminescence or absorbance measurements.[44,56−59] In addition, for bulk MoS_2, the temperature-dependent shift of −0.3 meV/K was shown to be mainly governed by electron−phonon interactions and not the thermal expansion of the lattice. We therefore expect the temperature-dependent shift of the exciton resonance in monolayers to be largely independent of the substrate.

The temperature increase ΔT extracted from the changes of the position and line width of the A exciton feature are presented in Figure 4 for a pump fluence of 101 $\mu J/cm^2$ using temperature coefficients of −0.3 (±0.1) meV/K to calculate the shift of the resonance energy and 0.15 (±0.05) meV/K for the increase in line width, respectively. The shaded areas are error bars corresponding to the maximum and minimum temperature coefficients from the literature. At short time delays after the excitation, the extracted values of ΔT from the line broadening and energy shift do not match, as expected, because the optical response in this regime is dominated by the presence of photoexcited carriers. For time delays greater than 10 ps, however, both the line broadening and the shift result in a similar estimate of the lattice temperature. Furthermore, this time scale corresponds to roughly twice the initial lifetime τ_{fast} of the optical response after the excitation, associated with the nonradiative decay of the charge carriers. Hence, after $2\tau_{fast} \approx$ 10 ps, as almost 90% of the photoexcited carrier population has decayed, presumably largely through Auger-type annihilation, the extracted lattice temperature reaches a maximum value ΔT_{max} as indicated in Figure 4(a). A comparison of the lattice temperature transients extracted from the shift of the resonance is further presented in Figure 4(b) for three different excitation fluences. We observe a linear scaling of the maximum temperature increase with the pump fluence and a similar time scale for the subsequent decay.

To estimate the expected temperature increase ΔT, we assume that the total absorbed energy of the pump pulse is converted into heat and use the relation $\Delta T = \Delta E/(d\rho c_p)$, where d = 0.618 nm denotes the thickness of the monolayer, ρ is the density of 7.5 g/cm^3, $c_p = 0.25\frac{J}{gK}$ is the heat capacity[60] of bulk WS_2, and ΔE is the absorbed pulse energy per area (using 5% absorption). The results of this estimate, presented in the inset of Figure 4(b) as a solid line, are in a good agreement with the maximum temperature jump extracted from analysis of the optical response. This finding strongly supports the assignment of the exciton line broadening and shift at longer time scales to an increase of the lattice temperature. In addition, the subsequent cooling of the lattice with a time constant on the order of 100 ps is largely consistent with the previous reports for supported atomically thin materials.[61] This rapid cooling is attributed to efficient transfer of heat from the sample to the underlying substrate. Using a simple model for heat conduction, we estimate the cooling rate under the assumption that the substrate acts as a cold reservoir and the heat flow is limited by the interfacial thermal conductance G.[62,63] In this case, the temperature of the WS_2 monolayer drops exponentially with a cooling time of $\tau_c = c_p\rho d/G$. The reported literature values for the interfacial thermal conductance at the van der Waals interface vary from 0.1 to several 10s of MW/(m^{2}K)[54,61,64,65] and yield τ_c in the range of a few 10s of picoseconds to several nanoseconds, in reasonable agreement with the measured cooling time. Thus, at longer time scales after the excitation (>10 ps), the temperature increase of the lattice and the subsequent cooling are sufficient to account for the pump-induced changes in the optical response, dominated by a red shift and line broadening of the exciton resonance.

The overall scenario after pulsed optical excitation of the WS_2 monolayer, consistent with our findings, is illustrated schematically in Figure 4(c) for the conditions of our measurements. Initially, electron−hole pairs are created by the pump pulse and induce a combination of bleaching and line broadening of the exciton resonance accompanied by a small blue shift in the energy of the resonance. The carrier population subsequently decays on a fast time scale, on the order of 5−15 ps, by efficient nonradiative decay dominated by Auger-type exciton−exciton annihilation. During this process, the energy is transferred from the carrier to the phonon system, resulting in a local temperature increase of the lattice and thus leading to an additional red shift of the exciton transition. At time delays greater than 10 ps after the excitation, the optical response remains dominated by the shift of the exciton resonance and residual line broadening. This remaining response decays on a time scale on the order of 100 ps, reflecting the cooling of the lattice by heat transfer from the monolayer to the underlying substrate. Although a small residual population of the photoexcited carriers might still be present in the system, the changes in the reflectance spectra at these time scales can be mostly accounted for simply by transient heating effects.

In summary, supported WS_2 monolayers have been studied by ultrafast white-light pump−probe spectroscopy at room temperature in a regime of intermediate excitation with injected electron−hole pair densities between 9×10^{11} and 1.3×10^{13} cm^{-2}. Transient spectra at the fundamental exciton transition were quantitatively analyzed by tracking individual contributions from the line broadening, bleaching, and an energy shift of

DOI: 10.1021/acs.nanolett.6b03513
Nano Lett. 2017, 17, 644−651

the resonance as a function of time delay after the excitation. The experimental results allow us to identify two main sources for the pump-induced changes of the optical response of the material. We observe interplay between modifications induced by many-body interactions from the photoexcited carrier population and by the subsequent transfer of excitation to the phonon system. In particular, transient heating of the lattice is found to be adequate to account for the pump-induced changes of the optical response on longer time scales.

AUTHOR INFORMATION

Corresponding Author

*E-mail: Claudia.ruppert@tu-dortmund.de.

ORCID

Claudia Ruppert: 0000-0001-9005-0420

Author Contributions

▽A.C. and C.R. contributed equally to this work.

Author Contributions

A.C. and C.R. designed the experiment, carried out the measurements, and analyzed the data. H.M.H. and A.F.R. prepared and characterized the samples. The manuscript was written through contributions of all authors. All authors have given approval to the final version of the manuscript.

Funding

This work was supported through the AMOS program at SLAC National Accelerator Laboratory within the Chemical Sciences, Geosciences, and Biosciences Division for data analysis. Sample preparation was by the Air Force Office of Scientific Research (grant FA9550-14-1-0268). A.C. gratefully acknowledges funding from the Deutsche Forschungsgemeinschaft (DFG) within the Emmy Noether Research Group program (CH 1672/1-1), from the Keck Foundation, and from the Alexander von Humboldt Foundation within the Feodor Lynen Research Fellowship program. H.M.H. and A.F.R. acknowledge funding from the National Science Foundation through the Integrated Graduate Education and Research Training Fellowship (DGE-1069240) and the Graduate Research Fellowship Program (DGE-1144155), respectively. C.R. gratefully acknowledges funding from the Alexander von Humboldt Foundation within the Feodor Lynen Research Fellowship program and by the collaborative research center SFB TRR142 of the DFG.

Notes

The authors declare no competing financial interest.

REFERENCES

(1) Novoselov, K. S.; Jiang, D.; Schedin, F.; Booth, T. J.; Khotkevich, V. V.; Morozov, S. V.; Geim, A. K. *Proc. Natl. Acad. Sci. U. S. A.* **2005**, *102* (30), 10451−10453.

(2) Mak, K. F.; Lee, C.; Hone, J.; Shan, J.; Heinz, T. F. *Phys. Rev. Lett.* **2010**, *105* (13), 136805.

(3) Splendiani, A.; Sun, L.; Zhang, Y.; Li, T.; Kim, J.; Chim, C.-Y.; Galli, G.; Wang, F. *Nano Lett.* **2010**, *10* (4), 1271−1275.

(4) Butler, S. Z.; Hollen, S. M.; Cao, L.; Cui, Y.; Gupta, J. A.; Gutiérrez, H. R.; Heinz, T. F.; Hong, S. S.; Huang, J.; Ismach, A. F.; Johnston-Halperin, E.; Kuno, M.; Plashnitsa, V. V.; Robinson, R. D.; Ruoff, R. S.; Salahuddin, S.; Shan, J.; Shi, L.; Spencer, M. G.; Terrones, M.; Windl, W.; Goldberger, J. E. *ACS Nano* **2013**, *7* (4), 2898−2926.

(5) Chhowalla, M.; Shin, H. S.; Eda, G.; Li, L.-J.; Loh, K. P.; Zhang, H. *Nat. Chem.* **2013**, *5* (4), 263−275.

(6) Xu, X.; Yao, W.; Xiao, D.; Heinz, T. F. *Nat. Phys.* **2014**, *10* (5), 343−350.

(7) Xia, F.; Wang, H.; Xiao, D.; Dubey, M.; Ramasubramaniam, A. *Nat. Photonics* **2014**, *8* (12), 899−907.

(8) Yu, H.; Cui, X.; Xu, X.; Yao, W. *Natl. Sci. Rev.* **2015**, *2* (1), 57−70.

(9) Mak, K. F.; Shan, J. *Nat. Photonics* **2016**, *10* (4), 216−226.

(10) Korn, T.; Heydrich, S.; Hirmer, M.; Schmutzler, J.; Schüller, C. *Appl. Phys. Lett.* **2011**, *99* (10), 102109−3.

(11) Wang, R.; Ruzicka, B. A.; Kumar, N.; Bellus, M. Z.; Chiu, H.-Y.; Zhao, H. *Phys. Rev. B: Condens. Matter Mater. Phys.* **2012**, *86* (4), 045406.

(12) Kumar, N.; He, J.; He, D.; Wang, Y.; Zhao, H. *J. Appl. Phys.* **2013**, *113* (13), 133702.

(13) Shi, H.; Yan, R.; Bertolazzi, S.; Brivio, J.; Gao, B.; Kis, A.; Jena, D.; Xing, H. G.; Huang, L. *ACS Nano* **2013**, *7* (2), 1072−1080.

(14) Cui, Q.; Ceballos, F.; Kumar, N.; Zhao, H. *ACS Nano* **2014**, *8* (3), 2970−2976.

(15) Wang, H.; Zhang, C.; Rana, F. *Nano Lett.* **2015**, *15* (1), 339−345.

(16) Moody, G.; Kavir Dass, C.; Hao, K.; Chen, C.-H.; Li, L.-J.; Singh, A.; Tran, K.; Clark, G.; Xu, X.; Berghäuser, G.; Malic, E.; Knorr, A.; Li, X. *Nat. Commun.* **2015**, *6*, 8315.

(17) Poellmann, C.; Steinleitner, P.; Leierseder, U.; Nagler, P.; Plechinger, G.; Porer, M.; Bratschitsch, R.; Schüller, C.; Korn, T.; Huber, R. *Nat. Mater.* **2015**, *14* (9), 889−893.

(18) Sim, S.; Park, J.; Song, J.-G.; In, C.; Lee, Y.-S.; Kim, H.; Choi, H. *Phys. Rev. B: Condens. Matter Mater. Phys.* **2013**, *88* (7), 075434.

(19) Kumar, N.; Cui, Q.; Ceballos, F.; He, D.; Wang, Y.; Zhao, H. *Phys. Rev. B: Condens. Matter Mater. Phys.* **2014**, *89* (12), 125427.

(20) Mouri, S.; Miyauchi, Y.; Toh, M.; Zhao, W.; Eda, G.; Matsuda, K. *Phys. Rev. B: Condens. Matter Mater. Phys.* **2014**, *90* (15), 155449.

(21) Sun, D.; Rao, Y.; Reider, G. A.; Chen, G.; You, Y.; Brézin, L.; Harutyunyan, A. R.; Heinz, T. F. *Nano Lett.* **2014**, *14* (10), 5625−5629.

(22) Singh, A.; Moody, G.; Wu, S.; Wu, Y.; Ghimire, N. J.; Yan, J.; Mandrus, D. G.; Xu, X.; Li, X. *Phys. Rev. Lett.* **2014**, *112* (21), 216804.

(23) Sie, E. J.; McIver, J. W.; Lee, Y.-H.; Fu, L.; Kong, J.; Gedik, N. *Nat. Mater.* **2015**, *14* (3), 290−294.

(24) Kim, J.; Hong, X.; Jin, C.; Shi, S.-F.; Chang, C.-Y. S.; Chiu, M.-H.; Li, L.-J.; Wang, F. *Science* **2014**, *346* (6214), 1205−1208.

(25) Steinhoff, A.; Rösner, M.; Jahnke, F.; Wehling, T. O.; Gies, C. *Nano Lett.* **2014**, *14* (7), 3743−3748.

(26) Chernikov, A.; van der Zande, A. M.; Hill, H. M.; Rigosi, A. F.; Velauthapillai, A.; Hone, J.; Heinz, T. F. *Phys. Rev. Lett.* **2015**, *115* (12), 126802.

(27) Pogna, E. A. A.; Marsili, M.; De Fazio, D.; Dal Conte, S.; Manzoni, C.; Sangalli, D.; Yoon, D.; Lombardo, A.; Ferrari, A. C.; Marini, A.; Cerullo, G.; Prezzi, D. *ACS Nano* **2016**, *10* (1), 1182−1188.

(28) Ulstrup, S.; Čabo, A. G.; Miwa, J. A.; Riley, J. M.; Grønborg, S. S.; Johannsen, J. C.; Cacho, C.; Alexander, O.; Chapman, R. T.; Springate, E.; Bianchi, M.; Dendzik, M.; Lauritsen, J. V.; King, P. D. C.; Hofmann, P. *ACS Nano* **2016**, *10* (6), 6315−6322.

(29) Chernikov, A.; Ruppert, C.; Hill, H. M.; Rigosi, A. F.; Heinz, T. F. *Nat. Photonics* **2015**, *9* (7), 466−470.

(30) Mannebach, E. M.; Li, R.; Duerloo, K.-A.; Nyby, C.; Zalden, P.; Vecchione, T.; Ernst, F.; Reid, A. H.; Chase, T.; Shen, X.; Weathersby, S.; Hast, C.; Hettel, R.; Coffee, R.; Hartmann, N.; Fry, A. R.; Yu, Y.; Cao, L.; Heinz, T. F.; Reed, E. J.; Dürr, H. A.; Wang, X.; Lindenberg, A. M. *Nano Lett.* **2015**, *15* (10), 6889−6895.

(31) Wang, Q.; Ge, S.; Li, X.; Qiu, J.; Ji, Y.; Feng, J.; Sun, D. *ACS Nano* **2013**, *7* (12), 11087−11093.

(32) Mai, C.; Barrette, A.; Yu, Y.; Semenov, Y. G.; Kim, K. W.; Cao, L.; Gundogdu, K. *Nano Lett.* **2014**, *14* (1), 202−206.

(33) Kumar, N.; He, J.; He, D.; Wang, Y.; Zhao, H. *Nanoscale* **2014**, *6* (21), 12690−12695.

(34) Zhu, C. R.; Zhang, K.; Glazov, M.; Urbaszek, B.; Amand, T.; Ji, Z. W.; Liu, B. L.; Marie, X. *Phys. Rev. B: Condens. Matter Mater. Phys.* **2014**, *90* (16), 161302.

(35) Dal Conte, S.; Bottegoni, F.; Pogna, E. A. A.; De Fazio, D.; Ambrogio, S.; Bargigia, I.; D'Andrea, C.; Lombardo, A.; Bruna, M.;

DOI: 10.1021/acs.nanolett.6b03513
Nano Lett. 2017, 17, 644−651

Ciccacci, F.; Ferrari, A. C.; Cerullo, G.; Finazzi, M. *Phys. Rev. B: Condens. Matter Mater. Phys.* **2015**, *92* (23), 235425.
(36) Yang, L.; Sinitsyn, N. A.; Chen, W.; Yuan, J.; Zhang, J.; Lou, J.; Crooker, S. A. *Nat. Phys.* **2015**, *11* (10), 830−834.
(37) Rivera, P.; Seyler, K. L.; Yu, H.; Schaibley, J. R.; Yan, J.; Mandrus, D. G.; Yao, W.; Xu, X. *Science* **2016**, *351* (6274), 688−691.
(38) Schmidt, R.; Berghäuser, G.; Schneider, R.; Selig, M.; Tonndorf, P.; Malić, E.; Knorr, A.; Michaelis de Vasconcellos, S.; Bratschitsch, R. *Nano Lett.* **2016**, *16* (5), 2945−2950.
(39) Li, Y.; Chernikov, A.; Zhang, X.; Rigosi, A.; Hill, H. M.; van der Zande, A. M.; Chenet, D. A.; Shih, E.-M.; Hone, J.; Heinz, T. F. *Phys. Rev. B: Condens. Matter Mater. Phys.* **2014**, *90* (20), 205422.
(40) Zhao, W.; Ghorannevis, Z.; Chu, L.; Toh, M.; Kloc, C.; Tan, P.-H.; Eda, G. *ACS Nano* **2013**, *7* (1), 791−797.
(41) Zeng, H.; Liu, G.-B.; Dai, J.; Yan, Y.; Zhu, B.; He, R.; Xie, L.; Xu, S.; Chen, X.; Yao, W.; Cui, X. *Sci. Rep.* **2013**, *3*, 1608.
(42) Currie, M.; Hanbicki, A. T.; Kioseoglou, G.; Jonker, B. T. *Appl. Phys. Lett.* **2015**, *106* (20), 201907.
(43) Mak, K. F.; He, K.; Lee, C.; Lee, G. H.; Hone, J.; Heinz, T. F.; Shan, J. *Nat. Mater.* **2012**, *12* (3), 207−211.
(44) Ross, J. S.; Wu, S.; Yu, H.; Ghimire, N. J.; Jones, A. M.; Aivazian, G.; Yan, J.; Mandrus, D. G.; Xiao, D.; Yao, W.; Xu, X. *Nat. Commun.* **2013**, *4*, 1474.
(45) Nie, Z.; Long, R.; Sun, L.; Huang, C.-C.; Zhang, J.; Xiong, Q.; Hewak, D. W.; Shen, Z.; Prezhdo, O. V.; Loh, Z.-H. *ACS Nano* **2014**, *8* (10), 10931−10940.
(46) Haug, H.; Koch, S. W. *Quantum theory of the optical and electronic properties of semiconductors*, 4th ed.; World Scientific, 2008.
(47) Jones, A. M.; Yu, H.; Ghimire, N. J.; Wu, S.; Aivazian, G.; Ross, J. S.; Zhao, B.; Yan, J.; Mandrus, D. G.; Xiao, D.; Yao, W.; Xu, X. *Nat. Nanotechnol.* **2013**, *8* (9), 634−638.
(48) Palummo, M.; Bernardi, M.; Grossman, J. C. *Nano Lett.* **2015**, *15* (5), 2794−2800.
(49) Wang, H.; Zhang, C.; Chan, W.; Manolatou, C.; Tiwari, S.; Rana, F. *Phys. Rev. B: Condens. Matter Mater. Phys.* **2016**, *93* (4), 045407.
(50) Amani, M.; Lien, D.-H.; Kiriya, D.; Xiao, J.; Azcatl, A.; Noh, J.; Madhvapathy, S. R.; Addou, R.; KC, S.; Dubey, M.; Cho, K.; Wallace, R. M.; Lee, S.-C.; He, J.-H.; Ager, J. W.; Zhang, X.; Yablonovitch, E.; Javey, A. *Science* **2015**, *350* (6264), 1065−1068.
(51) Liu, G.-B.; Shan, W.-Y.; Yao, Y.; Yao, W.; Xiao, D. *Phys. Rev. B: Condens. Matter Mater. Phys.* **2013**, *88* (8), 085433.
(52) Zhang, X.-X.; You, Y.; Zhao, S. Y. F.; Heinz, T. F. *Phys. Rev. Lett.* **2015**, *115* (25), 257403.
(53) Arora, A.; Nogajewski, K.; Molas, M.; Koperski, M.; Potemski, M. *Nanoscale* **2015**, *7* (48), 20769−20775.
(54) Cai, Y.; Lan, J.; Zhang, G.; Zhang, Y.-W. *Phys. Rev. B: Condens. Matter Mater. Phys.* **2014**, *89* (3), 035438.
(55) Sun, Q.-C.; Mazumdar, D.; Yadgarov, L.; Rosentsveig, R.; Tenne, R.; Musfeldt, J. L. *Nano Lett.* **2013**, *13* (6), 2803−2808.
(56) Zhao, W.; Ribeiro, R. M.; Toh, M.; Carvalho, A.; Kloc, C.; Castro Neto, A. H.; Eda, G. *Nano Lett.* **2013**, *13* (11), 5627−5634.
(57) Wang, G.; Bouet, L.; Lagarde, D.; Vidal, M.; Balocchi, A.; Amand, T.; Marie, X.; Urbaszek, B. *Phys. Rev. B: Condens. Matter Mater. Phys.* **2014**, *90* (7), 075413.
(58) Kobayashi, Y.; Sasaki, S.; Mori, S.; Hibino, H.; Liu, Z.; Watanabe, K.; Taniguchi, T.; Suenaga, K.; Maniwa, Y.; Miyata, Y. *ACS Nano* **2015**, *9* (4), 4056−4063.
(59) Selig, M.; Berghäuser, G.; Raja, A.; Nagler, P.; Schüller, C.; Heinz, T. F.; Korn, T.; Chernikov, A.; Malic, E.; Knorr, A. *Nat. Commun.* **2016**, *7*, 13279.
(60) O'Hare, P. A. G.; Hubbard, W. N.; Johnson, G. K.; Flotow, H. E. *J. Chem. Thermodyn.* **1984**, *16* (1), 45−59.
(61) Mak, K. F.; Lui, C. H.; Heinz, T. F. *Appl. Phys. Lett.* **2010**, *97* (22), 221904.
(62) Shenogin, S.; Xue, L.; Ozisik, R.; Keblinski, P.; Cahill, D. G. *J. Appl. Phys.* **2004**, *95* (12), 8136−8144.
(63) Hu, L.; Desai, T.; Keblinski, P. *Phys. Rev. B: Condens. Matter Mater. Phys.* **2011**, *83* (19), 195423.
(64) Liu, J.; Choi, G.-M.; Cahill, D. G. *J. Appl. Phys.* **2014**, *116* (23), 233107.
(65) Zhang, X.; Sun, D.; Li, Y.; Lee, G.-H.; Cui, X.; Chenet, D.; You, Y.; Heinz, T. F.; Hone, J. C. *ACS Appl. Mater. Interfaces* **2015**, *7* (46), 25923−25929.

DOI: 10.1021/acs.nanolett.6b03513
Nano Lett. 2017, 17, 644−651